THE ASTROPHYSICAL JOURNAL, 235:177–185, 1980 January 1

MASSES AND RADII OF WHITE-DWARF STARS. IV. THE TWO-COLOR DIAGRAM

HARRY L. SHIPMAN AND CHRISTINE A. SASS
University of Delaware
Received 1979 February 20; accepted 1979 July 9

ABSTRACT

Newly calculated model atmospheres, including both the effects of Lyman and Balmer line blanketing and the effects of convection, are used to determine the surface gravities of white-dwarf stars by the use of the separation of stars with different surface gravities in the Strömgren and multichannel two-color diagrams. The mean surface gravity of 40 stars in the appropriate temperature range with multichannel colors is $\log g = 8.04 \pm 0.25$, and the mean value for 35 stars with Strömgren photometry is $\log g = 7.86 \pm 0.25$. Comparison of all available investigations of white-dwarf masses shows that they are internally consistent with the possible exception of masses derived from gravitational redshifts, where a slight, marginally significant discrepancy may exist. The weighted mean of all mass determinations is 0.75 $M_\odot$, allowing for selection effects. The 1 σ range of white-dwarf masses extends from 0.5 $M_\odot$ to 1.0 $M_\odot$; we do not find evidence for a smaller mass range.

Subject headings: stars: atmospheres — stars: white dwarfs

I. INTRODUCTION

A determination of the mean mass of white-dwarf stars provides one key piece of information regarding the death of one class of stars. The degree of mass loss that precedes the white-dwarf stage can be evaluated, and an assessment of the role of white-dwarf stars in galactic evolution can be made, once the mean mass of white-dwarf stars is known. This paper completes a series of investigations of the mean masses of white-dwarf stars.

The application of model-atmosphere techniques to determinations of the mean radii, gravities, or masses of white-dwarf stars began several years ago. A variety of diagnostics have been applied to these objects, including colors for stars with parallaxes (Shipman 1972, hereafter Paper I), hydrogen line profiles (Paper I), and the two-color diagram (Wehrse 1975; Bessell and Wickramasinghe 1978; McGraw 1977). Paper II of this series (Shipman 1977) concerned the very cool hydrogen-rich stars; Paper III (Shipman 1979) used colors and photometry to determine radii for all white-dwarf stars with currently known parallaxes. This paper concerns the use of the two-color diagram, calibrated with the latest available model atmospheres, for the determination of surface gravities. Prior use of this technique was reported by Wehrse (1975), McGraw (1977), and Bessell and Wickramasinghe (1978).

Section II of this paper discusses the physical basis of the use of the two-color diagram in the determination of surface gravities, and the changes in the model atmosphere calibration of that diagram provided by the inclusion of both Lyman and hydrogen line blanketing and convection. The results from multichannel observations are also presented in § II and Figure 1. Gravity determinations from Strömgren photometry are discussed in § III, with the essential results shown in Figure 4. Section IV compares various methods of measuring white-dwarf masses, with summary tables provided as Tables 2 and 3.

II. THE TWO-COLOR DIAGRAM: SCANNER OBSERVATIONS

a) *Results of the Scanner Observations*

The two-color diagram for white-dwarf stars, where the multichannel color indices (Greenstein 1976) $u - v$ and $g - r$ are used as the axes, shows model atmospheres for white-dwarf stars falling along gravity-independent contours except in the range 7000 K $\lesssim T_{\rm eff} \lesssim$ 14,000 K (Fig. 1). In this temperature range, the $g - r$ color, measuring the slope of the Paschen continuum, is relatively independent of gravity while the $u - v$ color, measuring the Balmer jump, is dependent on gravity. Similar dependencies of color on gravity arise when other colors measuring the same physical quantities are plotted.

The gravity dependence of loci in the two-color diagram arises from the gravity dependence of the relative strength of bound-free atomic hydrogen and free-free H^- opacities in this temperature range. Since no physical explanation of this effect has (to our knowledge) appeared in the literature, it is worth a little exploration. The Balmer jump exists because most of the opacity in the Balmer continuum comes from atomic H bound-free absorption, which cuts off at the Balmer edge. Opacity in the Paschen continuum comes mostly from H^-. The ratio of these two opacity sources, the determinant of the size of the Balmer jump, obeys the scaling relation

$$\frac{\kappa_{H^-}}{\kappa_H} \sim \frac{n_{H^-}}{n_H} \sim \frac{n_H n_e}{n_H} \sim n_e \qquad (1)$$

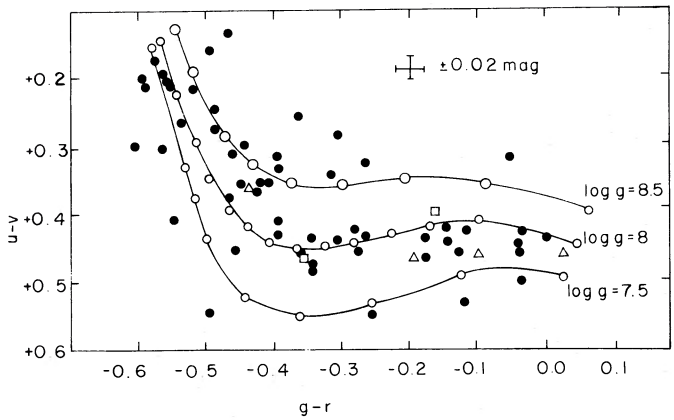

FIG. 1.—The multichannel two-color diagram for white-dwarf stars. Central wavelengths of the colors are 357 nm (u), 471 nm (g), 540 nm (v), and 694 nm (r). Dots denote observations (Greenstein 1976); circles are calculated values from ATLAS model atmospheres. Temperatures (in units of 10^3 K) are 8, 9, 10, 11, 12, 13, 13.5, 14, and 16 for $\log g = 7.5$; 8, 9, 9.5, 10, 10.5, 11, 11.5, 12, 12.5, 13, 13.5, 14, 15, and 16 for $\log g = 8$; and 8, 9, 10, 11, 12, 13, 14, 15, and 16 for $\log g = 8.5$. Squares are from Wickramasinghe's (1972) models, and triangles are from Wehrse's (1976) models. The Wehrse models include neither convection nor Lyman line blanketing.

when one considers the dependence of this ratio on electron density. The largest effect resulting from a change of 10 in g (or 1 in $\log g$) is an increase of the electron density at a particular optical depth in a white-dwarf atmosphere by a factor of 2 in the $T_{\rm eff}$ range considered here (7000 K–14,000 K). The T-τ relation is less dependent on gravity. As a result, when the gravity is increased, the H^- opacity, which does not change across the Balmer jump, becomes relatively more important. At high gravities, the opacities on either side of the Balmer jump are less unequal, the star looks more like a blackbody, the Balmer jump is smaller, and consequently the $u - v$ color is smaller. Detailed calculations bear out this argument and verify the scaling relation (1).

The model-atmosphere calculations used to calibrate the two-color diagram are from a detailed grid calculated recently. This grid will eventually be published in full; anyone desiring model details in advance of publication can obtain them from H. L. S. These models include Balmer line blanketing, Lyman line blanketing, and convection. Paper III contained a detailed discussion of the model physics, concluding that the model colors were accurate to 0.015 mag provided the physics is correct. These models are pure hydrogen models; such a chemical composition is expected to be representative for the DA stars. The principal uncertainty in the physics is the treatment of convection, an uncertainty which becomes more important at lower temperatures.

The determination of gravities from the two-color diagram is then rather straightforward. Observations from Greenstein (1976) were corrected to the Hayes-Latham calibration (Hayes and Latham 1975); a full discussion of calibration problems is provided in Paper III. The gravity of each star, listed in Table 1, is determined by interpolating between the loci of constant gravity in the diagram. Gravities were not determined for stars with $T_{\rm eff} \gtrsim 14{,}000$ K, since there the separation between lines of constant gravity becomes sufficiently small that accurate gravity determinations are not possible. Below $T_{\rm eff} = 8000$ K the model atmosphere grid becomes sparse, and this was then adopted as a lower limit to the temperature. The mean $\log g$ of 40 stars with multichannel colors is 8.04, with a standard deviation of the $\log g$ of each star of 0.47. The internal standard error of the mean value of $\log g$ of this sample is 0.07.

The external, true error of the mean surface gravity is probably much larger than the internal error. Uncertainties can arise from the fundamental calibration of the photometric system or from systematic uncertainties in the model atmosphere colors. Calibration of the photometric system was discussed extensively in Paper III; here we note that the uncertainty in the calibration of $u - v$ colors of 0.03 mag quoted by Hayes and Latham (1975) corresponds to an uncertainty in $\log g$ of 0.15 for the bulk of the temperature range considered here. Paper III also discussed the effects of uncertainties in the theory of convection, noting that decreasing the mixing length/pressure scale height ratio l/H, a conventional measure of convective efficiency, to 0.3 increased the $u - v$ color of a given model by 0.04 mag. Increasing the l/H value to 1.5 had no discernible effect. Since 0.04 mag corresponds to 0.2 in $\log g$, an uncertainty in the convective efficiency corresponds to another source of uncertainty in the surface gravity, although this uncertainty should only be applied in one direction. Were the convective efficiency, represented by the mixing length, overestimated, the presently derived gravities would be too small by 0.2 in the logarithm.

Combining these two sources of uncertainty—the absolute calibration and the effects of convection—produces a possible systematic uncertainty of 0.25 in $\log g$. This systematic uncertainty cannot be reduced by improvements in photometric accuracy since it comes from the calibrations. However, highly accurate

TABLE 1

TEMPERATURES AND SURFACE GRAVITIES

WD NUMBER	EG/GR/OTHER NUMBER	T MULTICHANNEL	G MULTICHANNEL	T STROMGREN	G STROMGREN	SOURCE OF STROMGREN PHOTOMETRY
0030+44	306	9.6	7.9			
0033+01	4	11.2	8.6			
0037-00				12.4	8.2	GREEN
0101+04	7	8.4	7.4	8.8	7.9	GREEN
0136+17				8.5	7.6	GREEN
0151+01	311	12.2	7.1			
0213+39	312	9.1	7.9			
0255-70	WEGNER 6			10.2	7.8	BW
0326-27	22			8.5	7.1	BW
0401+25	28	13.5	8.6	12.5	8.4	GRAHAM
0440+51	317	8.9	8.8			
0455+55	318	12.5	8.4			
0533+32	340	12.5	8.6			
0543+57	341	9.4	7.8			
0743+44	343	11.4	8.9			
0816+37	348	10.0	7.4			
0839-32	62			9.0	7.6	BW
0913+44	64			9.3	8.2	GRAHAM
0921+25	65	12.5	8.4			
0929-71	BPM 5639			9.2	7.6	BW
0930+29	324	8.3	8.0			
0935-37	66 N			8.4	8.1	BW
0939+07				9.2	7.7	GREEN
0950-57	WEGNER 14			12.0	7.7	BW
0955+24	69			8.6	7.8	GRAHAM
1015+07				8.5	7.6	GREEN
1052-08				9.9	7.4	GREEN
1055-07	74			8.0	7.8	GRAHAM
1055-07	74			8.1	7.7	GREEN
1108+56	351	8.9	7.2			
1147+25	84			10.6	8.2	GRAHAM
1159+80	355	11.4	8.0			
1236-49	WEGNER 22			10.0	8.3	BW
1244+14	92	10.4	8.1	11.2	8.4	GRAHAM
1253+48	357	13.6	8.4			
1257+27	94			8.6	7.7	GRAHAM
1327-08	99	12.8	9.0	15.4		GRAHAM(W 485)
1419+06				10.4	7.8	GREEN
1425-81	WEGNER 27=EG110			13.5	8.1	BW
1448+07	111	13.0	8.3			
1508+63	364	10.8	8.1			
1510+56	112	9.3	8.0			
1534+50	365	8.7	7.9			
1539-03	223			10.0	7.8	GRAHAM
1555-08	174			13.0	8.4	GRAHAM
1559+36	115	11.2	8.1	10.6	7.9	GRAHAM
1606+42	116			13.0	8.3	GRAHAM
1636+05	328	8.5	7.6			
1647+59	368	12.8	8.6			
1655+21B	197	9.4	7.9	9.7	7.8	GRAHAM
1706+33	198	13.1	8.1	11.5	8.3	GRAHAM
1716+02	123			12.3	8.3	GRAHAM
1736+05	371	8.7	7.7			
1840+04	225			8.2	7.7	GRAHAM
1857+12	128	10.5	8.1			
1950+25	394	12.0	8.2			
1953-01	135			8.0	7.4	GRAHAM
2025+48	396	10.5	7.9			
2105-82	WEGNER 37=EG142			9.7	7.6	BW
2115-56	WEGNER 38			9.2	7.7	BW
2116+67	300/400	13.5	7.0			
2149+37	401	12.6	7.7			
2240-01	154	9.1	7.7			
2246+22	155	10.5	8.6			
2311+55	404	11.1	7.8			
2326+04	159	11.9	8.1			
2341+32	162	12.5	8.3			
2347+12	405	11.1	7.8			
2359-48	165			8.4	7.4	BW

NOTE.—Temperatures are in units of 10^3 K; log g is in cgs units. The WD numbering system is that of the Villanova catalog (McCook and Sion 1977). EG/Gr numbers (EG for numbers less than 202 and Gr otherwise) are described in the references to Greenstein 1976, Wegner numbers are from Wegner 1973, and other designations can be found in Bessell and Wickramasinghe 1978 and Green 1977.

photometry would allow one to analyze differences in the gravities of these stars, permitting a more precise definition of the range of white-dwarf masses as well as an investigation of mass differences between different groups of stars (e.g., the variables and nonvariables).

b) Accuracy of the Model Atmospheres

Another possible source of uncertainty comes from the model-atmosphere calculations themselves. Figure 1 also includes model-atmosphere results from Wehrse (1975, 1976) and Wickramasinghe (Strittmatter and Wickramasinghe 1971; Wickramasinghe 1972). Neither of these calculations is strictly comparable to the calculations here, since the ATLAS models are the only set of the three which includes both hydrogen line blanketing (Balmer and Lyman lines) and convection. Wehrse included the Balmer lines but not the Lyman lines and neglected convection in most models. Wickramasinghe included Lyman line blanketing but also neglected convection. The present results, including both of these effects, should be more accurate.

Examination of Figure 1 shows essential agreement between Wickramasinghe's models (which have $\log g = 8$) and the ATLAS models, save that Wickramasinghe's are 0.05 mag redder in $g - r$ than the ATLAS models with similar temperatures. This difference is surprising in view of the successful comparison at higher temperatures (Paper III); the absolute flux level is also lower in the Wickramasinghe model, so any Wickramasinghe model does follow the H_V–$(g - r)$ relation of the ATLAS models within 1%; it looks like an ATLAS model that has a $T_{\rm eff}$ 500 K lower. This suggests that the difference is caused by the sparser frequency set used by Wickramasinghe to define the Lyman lines. An examination of Wickramasinghe's frequency set shows that line blanketing might have been underestimated, resulting in a higher integrated flux and thus a higher $T_{\rm eff}$ for a given model.

Figure 1 illustrates a considerable difference between the Wehrse (1975, 1976) models and the present ones. This difference can be attributed to Wehrse's neglect of convection and Lyman line blanketing and his inclusion of metal opacities with a metal abundance that now seems unrealistically high. Bessell and Wickramasinghe (1978) noted that a comparison of Strömgren colors with Wehrse's models showed an increase of $\log g$ with decreasing $T_{\rm eff}$. They suggested that changes in the H^- opacity or the addition of He to the atmosphere at low temperatures might cause this effect. Figure 2 shows that $\log g$ does not vary with T when the multichannel colors are used in the analysis; the effect noticed by Bessell and Wickramasinghe is not apparent when the models include all relevant energy transport mechanisms and opacities (particularly convection, which becomes important at low temperatures).

The appearance of Figure 2 strengthens the conclusions of Paper III regarding the accuracy of the models. Another supporting piece of information is provided by Figure 3, the high-temperature region of the multichannel two-color diagram. Here the theoretical locus from the model atmospheres is gravity-independent. If all models and observations are properly calibrated, the observations should follow the line. The composite hot white-dwarf star Feige 24 is not plotted and not included in this test, since the red companion is photometrically inseparable from the white-dwarf star. The mean deviation of the $g - r$ color from the line for the 25 stars with $T_{\rm eff} > 16{,}000$ K is $+0.0056 \pm 0.0082$ (observed minus calculated). The deviation of an individual observation is 0.041 mag, somewhat greater than the quoted errors of 0.02 mag for the colors. Since the observations follow the locus delineated by the models, this test shows that in this $T_{\rm eff}$ region, there is reason to believe that the models are correct and that the observations are properly calibrated.

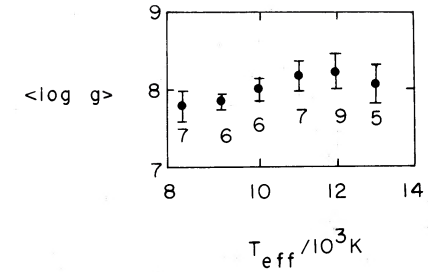

FIG. 2.—The mean gravity of stars in the sample in 1000 K intervals of $T_{\rm eff}$ plotted against $T_{\rm eff}$. There is no significant dependence of the mean gravity on $T_{\rm eff}$. Mean errors for the sample bins are shown.

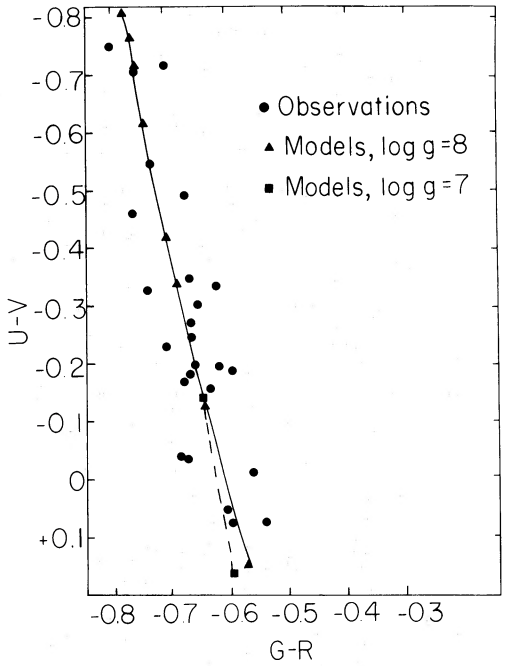

FIG. 3.—The multichannel two-color diagram at high temperatures, where the effects of gravity on the trajectory of stars in the diagram are minimal. The average concordance of models and observations supports the accuracy of the calibration.

III. STRÖMGREN PHOTOMETRY

The results of Paper III showed that Strömgren photometry, properly calibrated, is extremely useful for determining the atmospheric parameters of white-dwarf stars. While observations of stars in the critical temperature region where gravity determinations can be made from the two-color diagram are not extensive, they are sufficiently numerous and cover a different stellar sample from the sample of stars with published multichannel observations that a comparison with recent model atmospheres should be useful. The pioneering work in this area was that of Graham (1972), whose results were analyzed by Wehrse (1975) using model atmospheres having various shortcomings described in the previous section. Recently Bessell and Wickramasinghe (1978) published some Strömgren observations for southern-hemisphere white-dwarf stars, and Richard Green's thesis (1977) contains additional Strömgren data. Green has kindly made the results of his Strömgren photometry available prior to publication.

a) Results

It is thus both interesting and timely to evaluate white-dwarf gravities using this set of Strömgren photometry and model atmospheres that include all known relevant physical effects. Such a determination is illustrated in Figure 4, with the results presented in Table 1. The transformation from multichannel colors (or monochromatic flux ratios) to Strömgren colors was made using the empirically derived transformation formulae of Paper III. These transformations are strictly valid only for the Graham colors. Green (1977) and Bessell and Wickramasinghe (1978) argue that their observations are also on the Graham system.

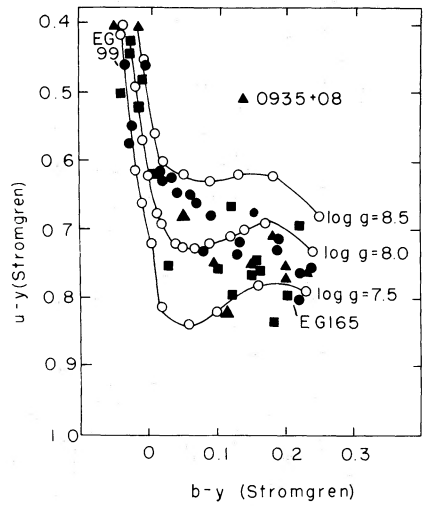

FIG. 4.—The two-color diagram in the Strömgren *uvby* system. *Circles and lines*, model-atmosphere colors. Filled symbols are observations: *triangles*, Green (1977); *squares*, Bessell and Wickramasinghe (1978); *dots*, Graham (1972). One errant point from Green's list is labeled with right ascension and declination. Two stars from the Eggen-Greenstein list, with possibly strange gravities from other methods, are also marked here; both seem normal.

Possible systematic errors introduced by the use of these transformations are discussed below.

Three individual stars in Figure 4 are noteworthy. One star from Green's list that falls far from the model lines is a star located at R.A. (1950) $09^h35^m02^s$, decl. (1950) 08°26′.8 N; this star was excluded from mean determinations of surface gravities. The photometry and spectrum classification of this star should be reexamined—it is classified as a DA; but if it is a DA, it is a rather strange one. A similarly errant point in the multichannel two-color diagram (Fig. 1) was EG 99 (= W485 A); its normal position in Figure 4 indicates that it is a normal star. It, too, will be excluded from the gravity comparisons which follow. EG 165 was noted in Paper III as having an abnormally small radius; its position in Figure 4 again provides no indication of a small radius (high gravity). The new photometry indicates that the temperature used in Paper III was much too high; the Paper III temperature was based on Johnson colors. The agreement of theory and observation in the upper left corner of Figure 4, where the locus defined by the models is gravity-independent, argues for the correctness of the calibration procedures in the same way that Figure 3 does.

The determination of a mean white-dwarf surface gravity from the data in Figure 4 requires one to use a high-temperature cutoff, since at high temperatures the two-color diagram becomes a less useful gravity discriminant. For the 35 determinations with $T_{\rm eff} <$ 14,000 K, the mean value of $\log g$ is 7.86 ± 0.06 (the error is the formal, internal, standard error of the mean value of $\log g$). However, the external error is likely to be considerably larger than the internal error, since the principal source of uncertainty is the fundamental calibration of the photometric system. A reasonable estimate is that the calibration uncertainty is the same as the calibration uncertainty for the multichannel system, 0.25 in $\log g$. Thus the mean surface gravity from Strömgren photometry should be quoted as $\langle \log g \rangle = 7.86 \pm 0.25$.

The Strömgren photometry used in this analysis comes from a variety of sources. The transformation formulae were derived for Graham's photometry, and are valid for the other sources only insofar as those sources are well tied to Graham's system. Mean values of $\log g$, with standard errors of the mean, determined from individual sources are: Graham, 16 stars, 8.03 ± 0.08; Bessell and Wickramasinghe, 11 stars, 7.72 ± 0.10; Green, 8 stars, 7.73 ± 0.08. The differences are not significant in view of the small numbers of stars in each sample. Green's photometry is not as accurate as photometry from the other two sources, since Green was seeking to separate DA's from DB's and to separate white-dwarf stars from other types of high-latitude blue objects.

b) Apparent Temperature Dependence of $\log g$ *in the Strömgren Two-Color Diagram*

Examination of Figure 4 shows that the gravity-finding method fails the test of Figure 2 when the

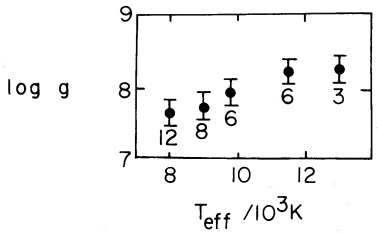

FIG. 5.—The mean gravity of stars determined from the Strömgren diagram as a function of $T_{\rm eff}$. Mean errors for the sample bins and the number of stars in each bin are shown. All sample intervals are 1000 K except for the one between 11,000 K and 13,000 K, where bins were combined to improve the statistics.

Strömgren colors are used. The mean value of $\log g$ decreases at low temperatures, in the opposite sense to the finding of Bessell and Wickramasinghe (1978) using the Wehrse (1975, 1976) models. Figure 5 is an analog of Figure 2, a plot of the mean value of $\log g$ for various $T_{\rm eff}$ ranges versus $T_{\rm eff}$. If all was well, there would be no dependence of $\langle \log g \rangle$ on $T_{\rm eff}$. The scatter in values of $\log g$ at an individual temperature is smaller in Figure 5 than in Figure 2; the observations show a narrower sequence in the Strömgren two-color diagram than in the multichannel two-color diagram, probably reflecting higher accuracies in the Strömgren colors. The nonconstancy of $\log g$ with $T_{\rm eff}$ shown in Figure 5 suggests that uncertainties still remain regarding the interpretation of the Strömgren colors.

Why don't the models reproduce the trajectory of the observations in the Strömgren two-color diagram, Figure 4? One can appeal to uncertainties in the transformation relations. The principal differences between the approach used here and in the parallel investigation by the Kiel group (Koester, Schulz, and Weidemann 1979) lies in the way that Strömgren colors are computed from the models. The Kiel group folded filter transmission functions with model-atmosphere fluxes to determine the shape of the relations between colors and atmospheric parameters and then folded scanner observations with transmission functions to determine zero points (Schulz 1978). In contrast, this work avoids using filter transmission functions entirely, using an empirical fit between multichannel and Strömgren colors to derive Strömgren colors for each model (Paper III). Both of these procedures have some uncertainties; the resulting loci in the Strömgren two-color diagram are not the same for the two sets of models. As a result of these problems, determinations of white-dwarf masses from Strömgren colors should be given lower weight.

Another source of uncertainty that should be mentioned is the models themselves. A convective efficiency of $l/H = 1$ has been assumed for these models. The limited set of numerical experiments reported in Paper III shows that setting $l/H = 0.3$ brings the 10,000 K models down 0.04 mag (redder in $u - v$) in the two-color diagram of multichannel colors, and a corresponding amount in the Strömgren diagram. This change produces higher values of $\log g$ for these stars, as desired to counteract the trend of Figure 5. Further exploration along these lines would be useful.

On balance, then, there are still some uncertainties to be cleared up regarding the interpretation of the Strömgren two-color diagram. If a fairly complete set of very accurate multichannel and Strömgren photometry in this region of the two-color diagram were available, the empirical fit of Paper III could be redone.

IV. COMPARISON OF DIFFERENT METHODS FOR MEASURING RADII

a) Mean Values

Table 2 provides a list of a number of determinations of mean masses of white-dwarf stars. The value provided by hydrogen line profiles in Shipman (1972) has been adjusted to allow for the effects of the new fundamental calibration of scanner observations by Hayes and Latham (1975); this correction reduces the

TABLE 2

WHITE-DWARF MASS DETERMINATIONS

Method (Reference)	No. of Stars	Result (mean value)	Mean Mass (raw data)	Corrected Mean Mass	Mass Range ($M/M_\odot$)
Photometry (Paper III)	110	$R/R_\odot = (1.27 \pm 0.06) \times 10^{-2}$	0.55	0.75 ± 0.06	Indeterminate
Photometry, $\Delta R/R < 0.1$ (Paper III)	31	$R/R_\odot = (1.20 \pm 0.08) \times 10^{-2}$	0.60	0.60 ± 0.08	0.22
Binary stars (notes)	7	$M/M_\odot = 0.73 \pm 0.08$	0.73	0.73 ± 0.08	0.23
Two-color diagram (multichannel; Fig. 1)	40	$\log g = 8.04 \pm 0.25$	0.60	0.80 ± 0.25	0.25:
Two-color diagram (Strömgren; Fig. 4)	35	$\log g = 7.86 \pm 0.25$	0.45	0.65 ± 0.25	0.15:
H-line profiles (Shipman 1972)	17	$\log g = 7.93 \pm 0.2$	0.55	0.75 ± 0.2	Indeterminate
Gravitational redshifts (Trimble and Greenstein 1972)	83	$k = 53$ km s^{-1}	0.8	1.0 ± 0.1	Indeterminate
Weighted mean				0.75	

NOTE.—The H-line profile results from Shipman (1972) have been corrected to allow for temperature adjustments arising from the Hayes and Latham (1975) recalibration of the absolute energy distribution of Vega. Binary star results are from Heintz 1974 (40 Eri B); Strand 1977 (Stein 2051 B); Strand 1951 (Procyon B); Young and Lanning 1975 (BD +16°516); Strand, Dahn, and Liebert 1976 (G107–70; two stars); and Gatewood and Gatewood 1978 (Sirius B).

mean value of log g by 0.08 because cooler temperatures are assigned to individual stars. Paper III showed that a magnitude-limited sample of white-dwarf stars will have a mean mass that is 0.2 solar masses less than the true mean white-dwarf mass because larger, less massive stars can be seen at greater distances, and thus a magnitude-limited sample will draw the low-mass stars from a larger volume of space than the high-mass stars. Corrections to allow for these selection effects have been applied to all mean radii except those determined from binary stars and from high-precision radii from Paper III. Stars with high-precision radii are generally those with large parallaxes, and applying a parallax cutoff provides a sample that is not limited by magnitude. While it is difficult to assess the possible influence of magnitude selection effects on the inclusion of particular stars in the small sample of white-dwarf stars in binary systems, it is reasonable to suspect that short-period binary systems would tend to be nearby (where the stellar separation is relatively large) and all white-dwarf stars, large and small, will be included in the sample. No correction for selection effects has been applied for the binary stars.

The columns in Table 2 are, for the most part, self-explanatory. The uncertainties quoted are all standard errors and include the contributions of systematic and random uncertainties. The Hamada-Salpeter (1961) mass-radius relation was used to translate measurements of R, log g, or gravitational redshift to mass measurements, and a carbon composition was assumed. (As long as white-dwarf stars are not made of hydrogen or iron, the interior composition has a very small effect on the mass-radius relation.) The last column contains an estimate of the range of masses covered by a particular sample and will be discussed in more detail in § IV*d*.

Table 2 indicates that almost all methods of measuring the mean mass of white-dwarf stars result in an answer that is consistent with the weighted mean of all methods of 0.75 solar masses, including a correction for selection effects. The higher mass provided by gravitational redshifts, discussed earlier in Paper I and by Trimble and Greenstein (1972), is still with us, as noted by Moffett, Barnes, and Evans (1978). However, the significance of this discrepancy has not grown and it may not even be real, as is discussed below. While the formal error of the weighted mean value is small, 0.05 $M_\odot$, the true uncertainty in the mean mass is somewhat larger because of a variety of possible systematic effects, particularly the uncertainties in the correction of 0.2 $M_\odot$ made to allow for selection effects. Thus the conclusions of Paper III are reinforced: the mean mass of white-dwarf stars is probably about 0.75 $M_\odot$. The principal uncertainty remaining at the present time is the uncertain correction for the tendency of magnitude-limited samples of stars to draw the stars with the largest radii (and smallest masses) from a larger volume of space.

One cautionary note should be applied concerning Table 2. The mean mass of white-dwarf stars in binary systems, while in agreement with the mean value derived from other samples, may represent a different sample of stars. Stars in binary systems can undergo mass exchange if the separation is small enough. One of the binaries has definitely undergone mass exchange, but BD +16°516 (= V471 Tau) has a mass of 0.7 $M_\odot$ and thus could be dropped from Table 2 without affecting the conclusions.

b) Comparison of Similar Samples

Do the various methods of measuring white-dwarf masses and radii really agree with each other? Figure 6 and Table 3 provide another approach to this question. Figure 6 is an up-to-date version of the mass-radius relation, with observations plotted according to the radius determinations of Paper III and masses determined only from binary star observations. The error boxes for the three systems with well-determined radii span 1 σ in each direction. Four stars (Procyon B, BD +16°516 = V471 Tau, and the two stars of G107–70) have radii that are not well determined, and so they are plotted along the horizontal axis only. Agreement between theory and current determination of masses and radii seems satisfactory. The position of 40 Eri B below the relations for $\mu = 2$ is intriguing but not significant.

Table 3 provides another approach. Here the mean radius, surface gravity, or mass of samples of stars which have been probed using two different methods of measuring the radius (or some equivalent parameter) are compared. Because the photometric method of radius measurement, used in Paper III, provided the most extensive sample, it was used as a benchmark to test various other methods. The uncertainties in Table 3 refer to internal errors—the standard deviation of the mean value of the difference between the two methods of measuring a particular quantity. Where radius

TABLE 3

COMPARISON OF METHODS OF MEASURING RADII

Method	No. of Stars in Common	(Difference Method) − (Photometric Method)
H-line profiles	13	$-0.16 \pm 0.12 = \Delta \log g$
Two-color diagram (multichannel)	18	$+0.11 \pm 0.09 = \Delta \log g$
Two-color diagram (Strömgren)	11	$+0.004 \pm 0.18 = \Delta \log g$
Binaries	6	$+0.13 \pm 0.12 = \Delta M/M_\odot$
Gravitational redshifts:		
Stars with known velocities	12	22 ± 12 km s^{-1} $= \Delta K$
All stars in common	23	13 km s^{-1} $= \Delta K$

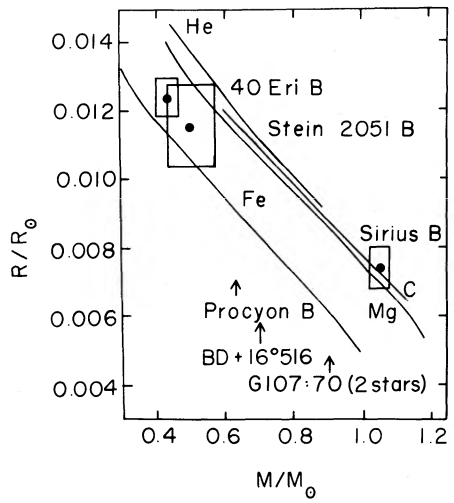

FIG. 6.—The mass-radius relation. *Lines*, theoretical relations of Hamada and Salpeter (1961). *Boxes*, binary stars with well-determined radii. *Arrows*, binary stars with poorly determined radii, where only the mass is shown.

values from Paper III had to be transformed to gravities or redshifts, carbon interiors were assumed. As long as the interiors are not hydrogen or some heavy element with the electron/nucleon ratio characteristic of iron, a different interior composition would not affect the results. All methods except possibly the gravitational redshift method agree with the radii of Paper III.

The general agreement between these various methods tends to support the assumption of carbon interior composition that has been commonly used for white-dwarf stars. However, the uncertainties are such that a precise determination of interior composition is really possible only for binary stars with well-determined masses (Liebert 1976; Gatewood and Gatewood 1978). Investigation of Sirius B (Greenstein, Oke, and Shipman 1971; Gatewood and Gatewood 1978) shows that compositions of Fe or H can be definitely excluded. The situation is less clear for 40 Eri B or Stein 2051 (Liebert 1976).

c) Gravitational Redshifts

There is a difference between the mean mass of white-dwarf stars determined from gravitational redshifts and from other methods (Tables 2 and 3). This difference was noticed several years ago (Paper I; Trimble and Greenstein 1972). In Table 3, the gravitational redshift measurement is compared to the photometric method in two ways. Twelve stars can have gravitational redshifts measured in an absolute sense, since these stars are in stellar systems and their radial velocities can therefore be considered known. This list of 12 stars was confined to stars with low-dispersion measurements of gravitational redshifts in the interests of having a uniform sample. Individual, higher-precision measurements of three particular stars, Sirius B (Greenstein, Oke, and Shipman 1971; Gatewood and Gatewood 1978), 40 Eri B (Greenstein and Trimble 1972), and CoD $-38°10980$ (Wegner 1978) show essential agreement between the redshift measurement and other methods of determining the stellar radius and mass. The uncertainty listed in Table 2 is a 1 σ error, so that the statistical significance of the difference is marginal. Further, there is a sample of 23 stars with radii calculated in Paper III where their true radial velocities are not known. One can apply the same statistical technique to this sample that Trimble and Greenstein (1972) applied to their larger sample: presume that an average positive value for the radial velocity corresponds to a gravitational redshift. A predicted mean redshift for these stars, using radii from Paper III and the Hamada-Salpeter (1961) mass-radius relation, is 25 km s^{-1}; the actual, observed value is 38 km s^{-1}, 13 km s^{-1} larger than the value predicted by the photometric radii. The significance of this difference is hard to evaluate.

In the past, it has been asserted that pressure shifts could contribute to the discrepancy between predicted and observed gravitational redshifts (Wiese and Kelleher 1971). Shipman and Mehan (1976) showed that the effects of pressure shifts alone are quite small, and this conclusion was confirmed by Schulz (1977), despite the statement in Schulz's abstract that his results contradict ours. What Schulz did show was that a monotonic dependence of photographic density on wavelength—a continuum slope—could result in observational errors when a Grant measuring engine was used. The possible influence of this effect had been mentioned earlier by Greenstein and Trimble (1967). Whether the continuum slope problem plays a role depends on the techniques used for gravitational redshift measurement. The Sirius B measurement (Greenstein, Oke, and Shipman 1971) explicitly allowed for this effect, and the measurement of gravitational redshifts from narrow cores (Greenstein *et al.* 1977) is also not affected by continuum slope. The difference of -3.6 ± 4.7 km s^{-1} between low-dispersion and narrow-core measurements, noted by Greenstein *et al.* (1977), tends to argue against the idea that continuum slope significantly ($\gtrsim$10 km s^{-1}) affects low-dispersion measurements. Thus the present results show that (i) neither pressure shifts nor continuum slope effects nor consideration of a more extensive sample have made the slight discrepancy between gravitational redshift measurements and other methods of determining white-dwarf masses go away but that (ii) the significance of this difference is still marginal.

d) Mass Ranges

Table 2 lists a number of values for the mass range of various samples of white-dwarf stars. These ranges are determined from the following relation between σ (the actual dispersion of a sample of stars), $\sigma_{\rm obs}$ (the dispersion expected from the known observational uncertainties), and $\sigma_{\rm sample}$ (the dispersion of the sample observations):

$$\sigma^2 = \sigma^2_{\rm sample} - \sigma^2_{\rm obs} . \qquad (2)$$

Equation (2) was applied to the property (radius, mass, or surface gravity) measured by each method, and the resulting dispersions were converted to mass dispersions via the mass-radius relation.

The two best-determined mass ranges in Table 2 are those where σ_{obs} is reasonably well known and smaller than σ_{sample}: the binary stars and the high-precision sample from Paper III. While the uncertainties in the masses of binary stars are sometimes very small indeed, there is always the possibility that mass exchange has affected the past evolution of some of them. The photometric radius measurements in Paper III were made via a surface-brightness method, a method which has the virtue of explicitly stating the source of errors. For the 31 high-precision stars, the dispersion expected from observations is $\sigma_{obs}(R)/R = 0.079$, one-third of the sample spread $\sigma_{sample}(R)/R = 0.23$. The uncertainties of Paper III would have to be 2.7 times as large as they are claimed to be if the width of the white-dwarf mass distribution, expressed as $\sigma(M)$, were to have the value of 0.1 $M_\odot$ quoted by Koester *et al.* (1979).

It is less easy to determine the width of the white-dwarf mass distribution using data from the two-color diagram. Uncertainties of 0.04 mag in the observed colors were adopted to obtain the mass ranges listed in Table 2. The mass range determined from this method is extremely sensitive to the adopted uncertainties in the photometry. Further, the samples of stars with suitable Strömgren or multichannel colors published in the literature are small. Were a larger sample of data, with small ($\sim$0.01 mag), well-determined uncertainties, available, it might be possible to obtain another estimate of the width of the white-dwarf mass distribution.

V. SUMMARY

The essential results of this paper are:

1. The mean surface gravity of 40 white-dwarf stars, derived from multichannel observations and the two-color $(u - v, g - r)$ diagram, is 8.04 ± 0.25.
2. The mean surface gravity of 35 stars with Strömgren colors, using the Strömgren $(u - y, b - y)$ diagram, is 7.86 ± 0.25.
3. A wide variety of methods indicate that the mean mass of white-dwarf stars in the Galaxy is 0.75 $M_\odot$, taking selection effects into account.
4. Comparison of different methods of measuring the masses of white-dwarf stars shows consistency among all methods. There is a slight discrepancy between measurements of gravitational redshifts and other methods; the significance of this discrepancy is unclear, and it may well not be real.

We thank the National Science Foundation for financial support, Gary Wegner for useful discussions, and Richard Green and Volker Weidemann for communicating results prior to publication. An anonymous referee provided helpful suggestions.

REFERENCES

Bessell, M. S., and Wickramasinghe, D. T. 1978, *M.N.R.A.S.*, **182**, 275.
Gatewood, G., and Gatewood, C. 1978, *Ap. J.*, **225**, 191.
Graham, J. 1972, *A.J.*, **77**, 144.
Green, R. 1977, Ph.D. thesis, California Institute of Technology.
Greenstein, J. L. 1976, *A.J.*, **81**, 323.
Greenstein, J. L., Boksenberg, A., Carswell, R., and Shortridge, K. 1977, *Ap. J.*, **212**, 186.
Greenstein, J. L., Oke, J. B., and Shipman, H. L. 1971, *Ap. J.*, **169**, 563.
Greenstein, J. L., and Trimble, V. 1967, *Ap. J.*, **149**, 283.
———. 1972, *Ap. J. (Letters)*, **175**, L1.
Hamada, T., and Salpeter, E. E. 1961, *Ap. J.*, **134**, 683.
Hayes, D. S., and Latham, D. W. 1975, *Ap. J.*, **197**, 593.
Heintz, W. D. 1974, *A.J.*, **79**, 819.
Koester, D., Schulz, H., and Weidemann, V. 1979, *Astr. Ap.*, in press.
Liebert, J. W. 1976, *Ap. J.*, **210**, 715.
McCook, G. P., and Sion, E. M. 1977, *Villanova Obs. Contr.*, No. 2.
McGraw, J. T. 1977, Ph.D. thesis, University of Texas at Austin.
Moffett, T. J., Barnes, T. G., III, and Evans, D. S. 1978, *A.J.*, **83**, 829.
Schulz, H. 1977, *Astr. Ap.*, **54**, 315.
———. 1978, *Astr. Ap.*, **68**, 75.
Shipman, H. L. 1972, *Ap. J.*, **177**, 723 (Paper I).
———. 1977, *Ap. J.*, **213**, 138 (Paper II).
———. 1979, *Ap. J.*, **228**, 240 (Paper III).
Shipman, H. L., and Mehan, R. G. 1976, *Ap. J.*, **209**, 205.
Strand, K. Aa. 1951, *Ap. J.*, **113**, 1.
———. 1977, *A.J.*, **82**, 745.
Strand, K. Aa., Dahn, C. C., and Liebert, J. W. 1976, *Bull. AAS*, **8**, 506.
Strittmatter, P. A., and Wickramasinghe, D. T. 1971, *M.N.R.A.S.*, **152**, 47.
Trimble, V., and Greenstein, J. L. 1972, *Ap. J.*, **177**, 441.
Wegner, G. A. 1973, *M.N.R.A.S.*, **163**, 381.
———. 1978, *M.N.R.A.S.*, **182**, 111.
Wehrse, R. 1975, *Astr. Ap.*, **59**, 169.
———. 1976, *Astr. Ap. Suppl.*, **24**, 95.
Wickramasinghe, D. T. 1972, *Mem. R.A.S.*, **76**, 129.
Wiese, W. L., and Kelleher, D. E. 1971, *Ap. J. (Letters)*, **166**, L59.
Young, A., and Lanning, H. H. 1975, *Pub. A.S.P.*, **87**, 461.

HARRY L. SHIPMAN: Physics Department, University of Delaware, Newark, DE 19711
CHRISTINE A. SASS: Hewlett-Packard Company, Avondale, PA 19311